Supporting Information Appendix for

"Visualizing Long-Term Single-Molecule Dynamics *in vivo* by Stochastic Protein Labeling"

Table of Contents:

SUPPLEMENTARY FIGURES

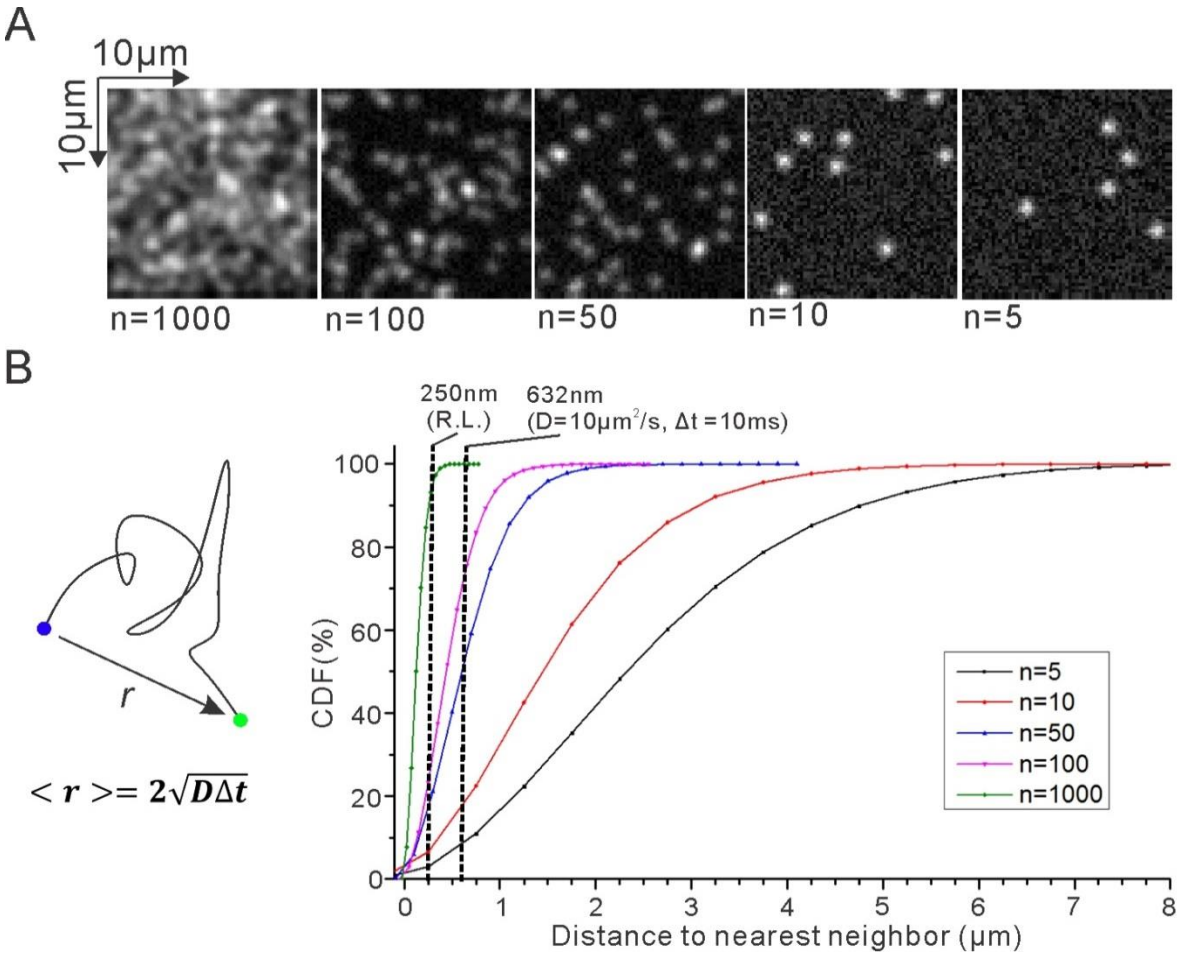

Fig. S1. Sparse labeling is essential for reliable single-molecule localization and tracking

(*A*) Uniformly distributed single molecule images in a 10 μm by 10 μm square area, similar to the size of a mammalian cell nucleus. N indicates the number of single molecules in each image. See *Supplementary Methods* and **Eqn. S9 - S11** for detailed parameters for the simulation.

(*B*) Left: When one molecule undergoes Brownian diffusion with a diffusion coefficient of D, the molecule expects to jump a distance of <r> between two frames with a temporal delay of Δt. For example, when D = 10 $\mu m^2/s$ and Δt = 10 ms, the expected distance between two frames <r> = 632 nm.

Right: For each condition indicated in (*A*), the distance to the nearest neighbor for each molecule was calculated and distances for all molecules were pooled to generate the cumulative distribution function (CDF) curve. R.L. indicates the resolution limit (~250 nm). When molecules are densely packed above a density of 10^2 ~ 10^3 per cell, increasingly more molecules cannot be unambiguously localized, due to overlaps between single molecule images. Likewise, when the packing density is above 10 ~ 10^2 per cell, accurate tracking cannot be performed because of interferes from nearby molecules.

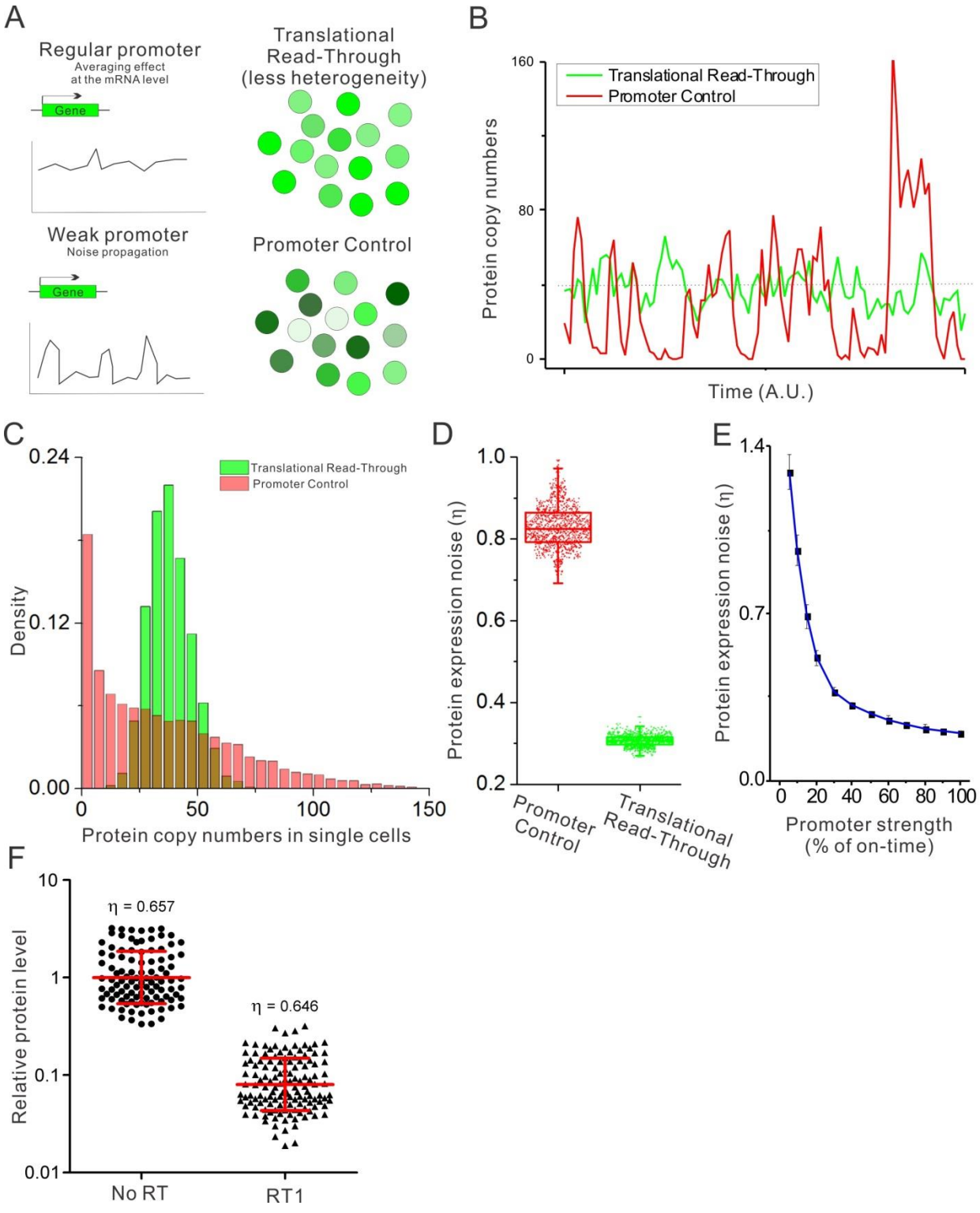

Fig. S2. Sparse labeling with translational read-through gives rise to less labeling heterogeneity

(*A*) Schematics illustrating single cell gene expression heterogeneity.

Upper panel: the RT strategy enables sparse labeling with low gene expression noise because of averaging effect from the high copy number of mRNA molecules in the cell.

Bottom panel: Due to the low copy number of DNA molecules in the cell and the bursting kinetics of transcription, weak promoters tend to give rise to high gene expression noise.

(*B*) When the average protein copy numbers in the cell are the same, promoter control gives rise to higher temporal variations in gene expression, compared to a RT strategy. See *Supplementary Methods* for detailed simulation parameters.

(*C*) Protein copy number histogram in single cells, comparing a weak promoter strategy (Light red) with a RT strategy (Green). See *Supplementary Methods* for detailed simulation parameters.

(*D*) Protein expression noises for promoter control (Red) and RT (Green) condition for data presented in (*C*), based on 1000 simulations. Here we define the protein noise (η) as the standard deviation divided by the mean. In the box chart, top and bottom error bars represent 95% and 5% percentile, respectively; triangle represents the range from 25% to 75% percentile; center line represents the median and the small square represents the mean value.

(*E*) Protein expression noise as the function of promoter strength. See *Supplementary Methods* for detailed simulation parameters.

(*F*) Comparison of mEOS4b protein expression noise between EF1-H2B-mEOS4b (No RT) and EF1-H2B-RT1-mEOS4b (RT1) in U2OS cells. The data points indicate the relative mEOS4b green fluorescent intensities (normalized to No RT condition) in positively transfected cells. Protein expression noise (η) could be calculated from original fluorescent intensity data.

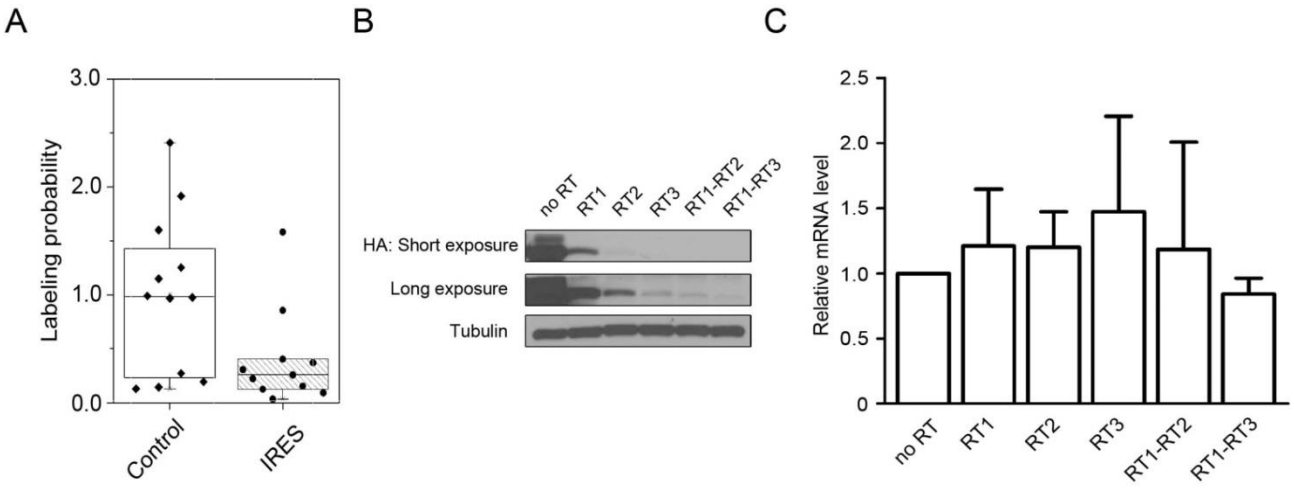

Fig. S3. RT strategy is an efficient approach for labeling density control

(*A*) Labeling density reduction by IRES. IRES was placed in front of H2B-mEOS4b-HA and then live-PALM experiments were performed to estimate localization densities in single cells. H2B-mEOS4b localization densities in IRES condition (n = 11 cells) were normalized to the average density in no IRES control (n = 12 cells). Error bars represent SD.

(*B*) Western blot analysis of RT efficiencies for different RT sequences as indicated above each lane. H2B and mEOS-HA are separated by different RT sequences as shown in **Fig. 1** ***B*** and ***C***. 48 hours after transfection in U2OS cells, anti-HA western blot experiment was performed to examine H2B-mEOS-HA fusion protein levels.

(*C*) Quantitative PCR analysis of mRNA expression levels in different RT conditions in U2OS cells. Error bars reflect SD. (*B*) and (*C*) are from three independent biological replicates. All constructs from (*A*), (*B*), and (*C*) are under the control of EF1 promoter.

A

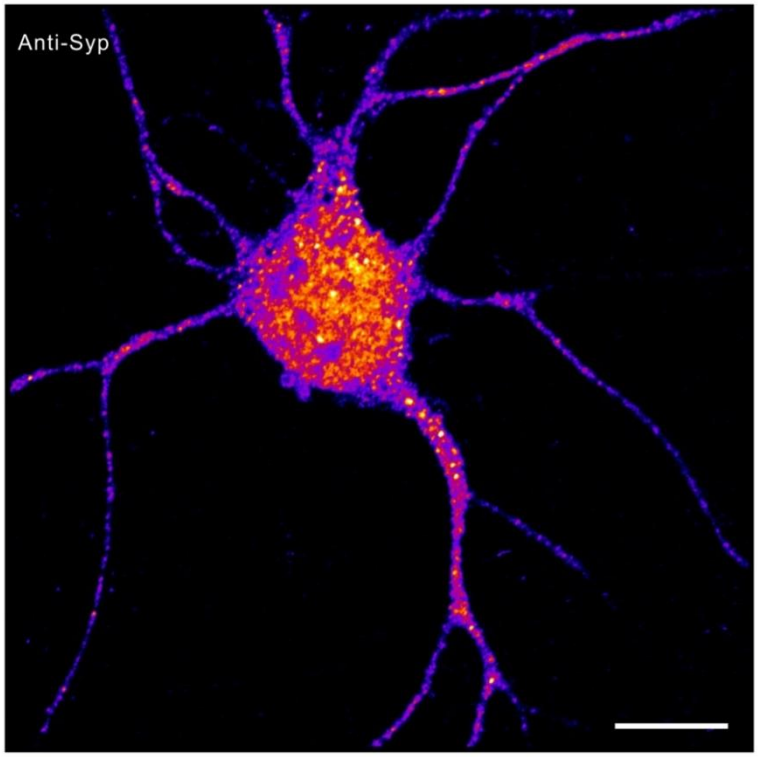
Anti-Syp

B

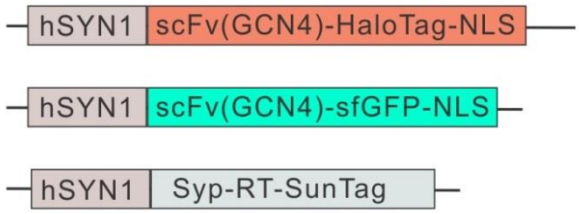
hSYN1
scFv(GCN4)-HaloTag-NLS
hSYN1
scFv(GCN4)-sfGFP-NLS
hSYN1
Syp-RT-SunTag

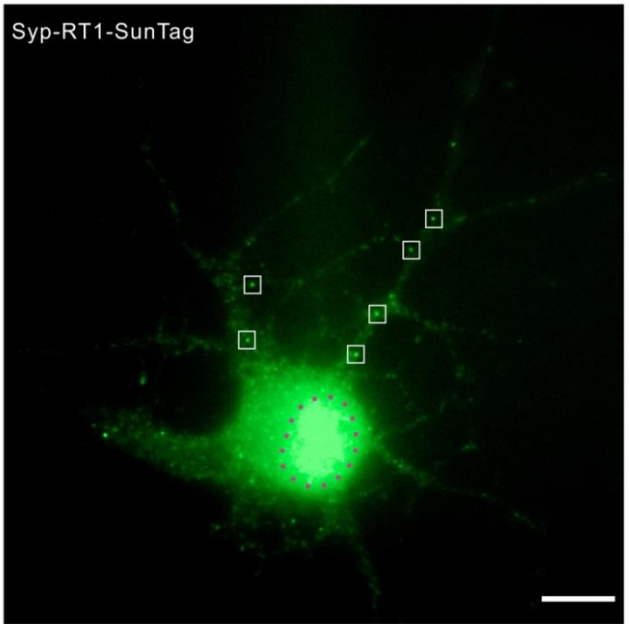
Syp-RT1-SunTag

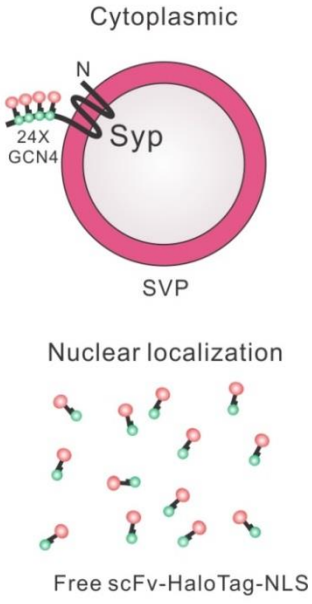
Cytoplasmic
N
24X
GCN4
Syp
SVP
Nuclear localization
Free scFv-HaloTag-NLS

Fig. S4. Sparse labeling of densely packed SVPs/SVs

(*A*) Synaptophysin immune-fluorescence staining (Airyscan imaging) in DIV 6 cultured hippocampal neurons shows high SVP/SV packing densities in soma and neurites. See *Supplementary Methods* for staining and imaging details.

(*B*) Upper panel: constructs for the Syp-RT-SunTag labeling. The expression of all the components is driven by a neuron-specific promoter from human synapsin gene (hSyn1). The NLS facilitates the nuclear import of free single chain antibodies, reducing fluorescence background in the cytoplasm.

Lower, a representative image acquired by highly-inclined and laminated optical sheet (HILO) illumination (1) showing sparse SVP/SV labeling (RT2) in a hippocampal neuron. White boxes highlight SVPs/SVs labeled by the SunTag. Enrichment of fluorescence signals in the nucleus (dotted red circle) reflects nuclear localization of free scFv-HaloTag (JF549) –NLS molecules.

Scale bar: 10 µm

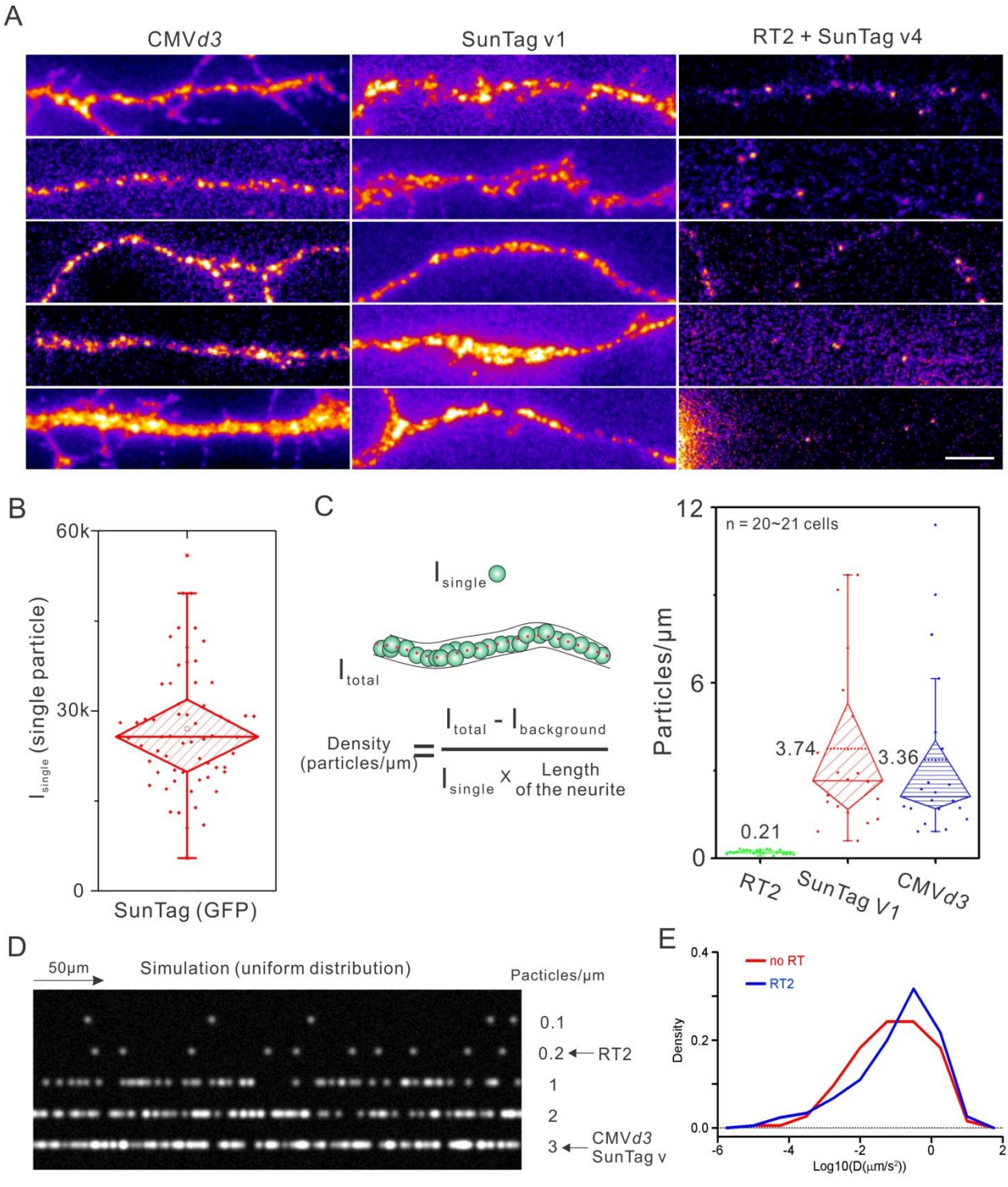

Fig. S5. Labeling density comparison with CMV*d3,* SunTag v1 and the RT strategy

(*A*) Representative cells (n = 5) for each labeling condition - CMV*d3* (left), SunTag v1 (middle) and the RT strategy (right). CMV*d3* was used as the promoter for Syp-SunTag v4 expression.

The hSyn1 promoter was used for the Syp-SunTag v1 expression same as the RT condition. See **Movie S4** for details. Scale bar: 5 μm

(*B*) Single-molecule intensity (I_{single}) for synaptic vesicles labeled by Syp-SunTag (GFP) calculated using data in the RT condition (n = 63). Specifically, I_{single} is the sum of intensity values from pixels in a single-molecule image subtracted by the background intensity derived from a control region. See *Supplementary Methods* for calculation details. In the box chart, top and bottom error bars represent 95% and 5% percentile, respectively; triangle represents the range from 25% to 75% percentile; center line represents the median and the small square represents the mean value.

(*C*) Labeling density statistics for each labeling condition.

Left, Schematics showing that the labeling density (particles/μm) is defined as the total intensity ($I_{total} - I_{background}$) in the neurite divided by the average single particle intensity (I_{single}) and then by the length of the neurite.

Right, particle densities calculated for each condition (n = 20 ~ 21 cells). In the box chart, top and bottom error bars represent 95% and 5% percentile, respectively; triangle represents the range from 25% to 75% percentile; center line represents the median and the dotted line represents the mean value (labeled).

(*D*) Simulated image showing the effects of labeling density on single-molecule imaging. Specifically, single molecules were randomly placed along linear neurites (50 μm) at different densities. Single molecule images start to overlap with each other above 1 particles/μm. See *Supplementary Methods* and **Eqn. S9** and **S10** for simulation details.

(*E*) Density histogram of log10 (Diffusion coefficient) for the trajectories from SunTag-labeled Syp without (no RT) or with RT2 sequence. Because of the dense labeling, single synaptic

vesicles in no RT condition were hard to be resolved and displayed slower movement comparing to that in RT2 condition. Acquisition rate: 50 Hz

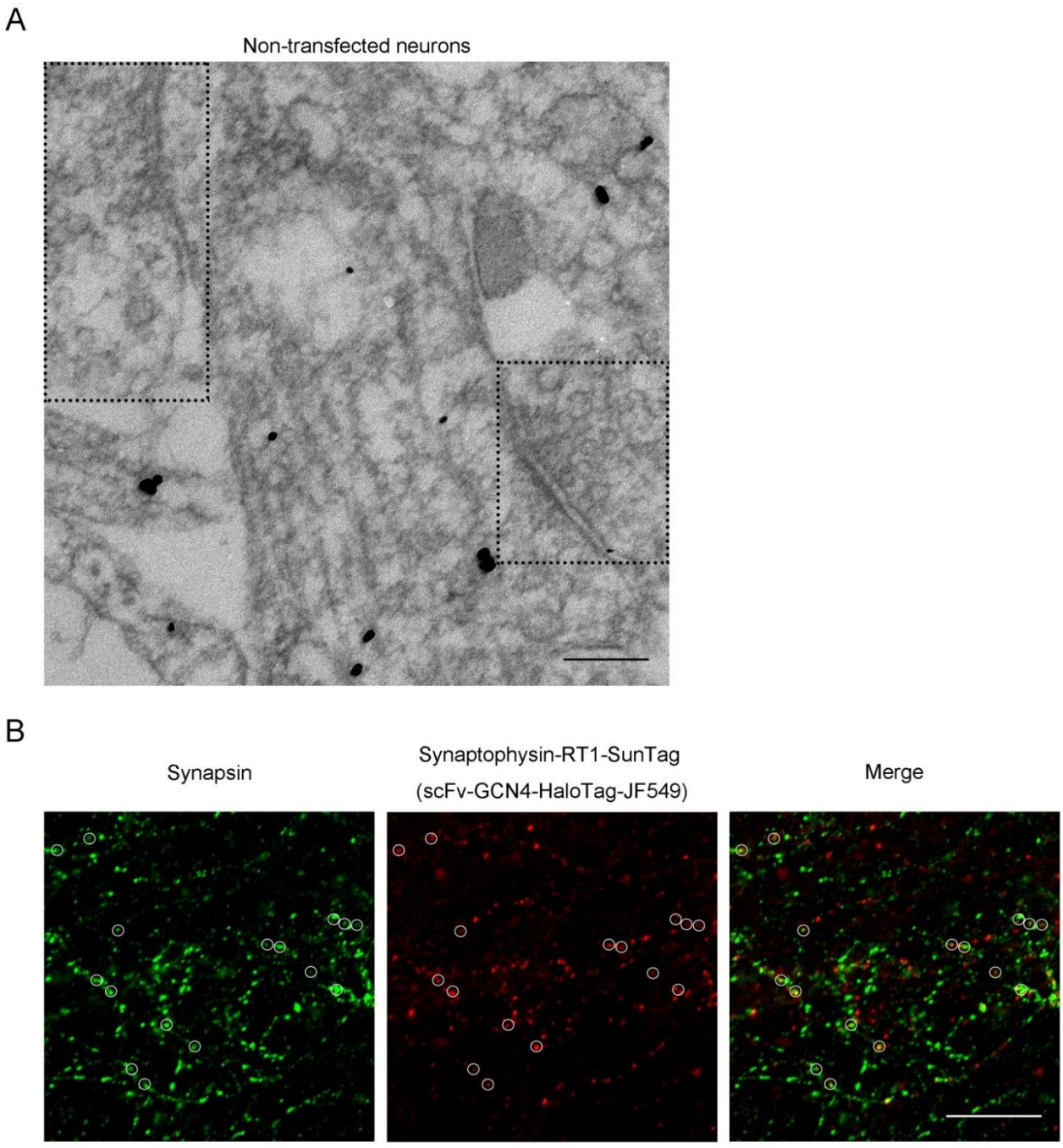

Fig. S6. Targeting of SunTag labeled SVPs/SVs to synapses.

(*A*) Representative immuno-EM images of non-transfected DIV 12 hippocampal neurons showing sparse, non-specific signals outside of the synapse regions indicated by the dotted black boxes. Scale bar: 200 nm

(*B*) SVPs/SVs sparsely labeled (RT1) by Syp-SunTag (scFv–HaloTag–JF549) were targeted to pre-synaptic regions (labeled with Synapsin, Airyscan imaging). Co-localization events were indicated by white circles. The Syp fluorescent signals that are not localized with Synapsin likely reflect SVPs transported in the neurites. Scale bar: 10 μm

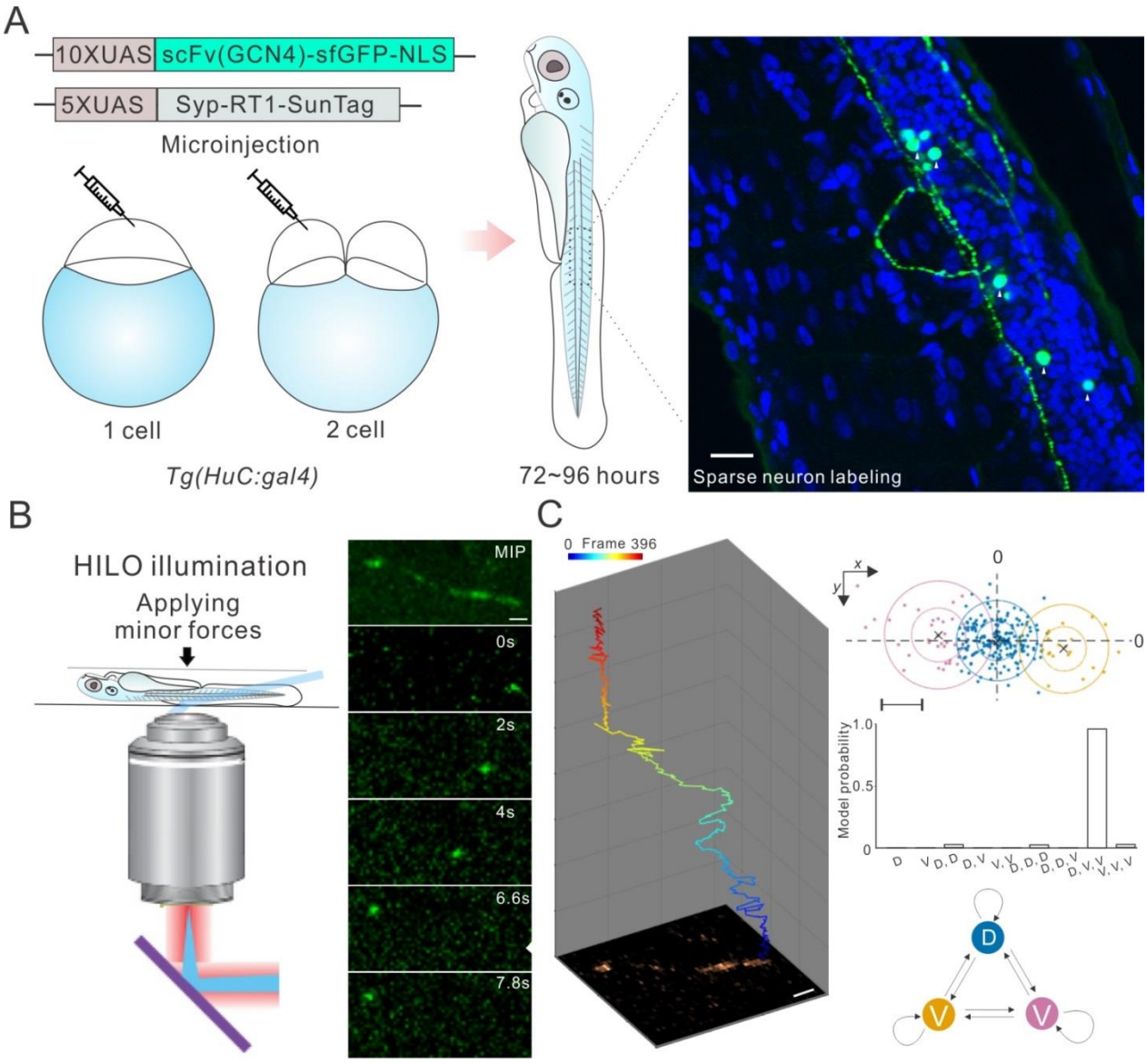

Fig. S7. Imaging SVP/SV dynamics in *zebrafish*

(*A*) Left: Two constructs encoding Syp-SunTag (GFP) components were microinjected into *Tg(HuC:gal4) zebrafish* embryos at one or two cell stage. Specifically, the HuC promoter drives pan-neuronal expression of transcription activator (gal4). Right. Three days after microinjection, samples were fixed and confocal imaging was performed to evaluate labeling efficiency. Note, due to stochastic genome integration, only a small fraction of neurons expressed the Syp-

SunTag (GFP: Green) system (indicated by white arrows). SVPs/SVs in the axons of the spinal cord regions are also labeled. Nuclei were counterstained with DAPI. Scale bar: 20 μm

(*B*) Left, Schematics explaining SVP/SV imaging in *zebrafish*. The *zebrafish* sample was placed between two cover-glasses. Minor forces were applied to keep the sample still and physically close to the cover glass. HILO illumination was induced by having the illumination laser with an incident angle slightly smaller than the critical angle. See **Movie S5** for details. Acquisition rate: 50 Hz

Right, one SVP moving along the neurite. The maximal intensity projection (MIP) image was shown on the top. Raw live image frames were shown below. Scale bar: 1 μm

(*C*) Left, a representative SVP trajectory consists of 396 frames showing dynamic transitions between diffusion and active transport states. See **Movie S6** for the raw imaging data. The frame number is color-coded as indicated by the color bar above. Scale bar: 1 μm

Right-top, displacements between frames for the trajectory can be classified by the HMM-Bayes algorithm into one diffusion state (blue) and two transport states with opposing directions (yellow; pink). Right-middle, the probabilities of competing models for correctly describing the hidden states in the trajectory. Right-bottom, hidden Markov model diagram describing the dynamic behavior of SVP in the trajectory. Scale bar: 200 nm

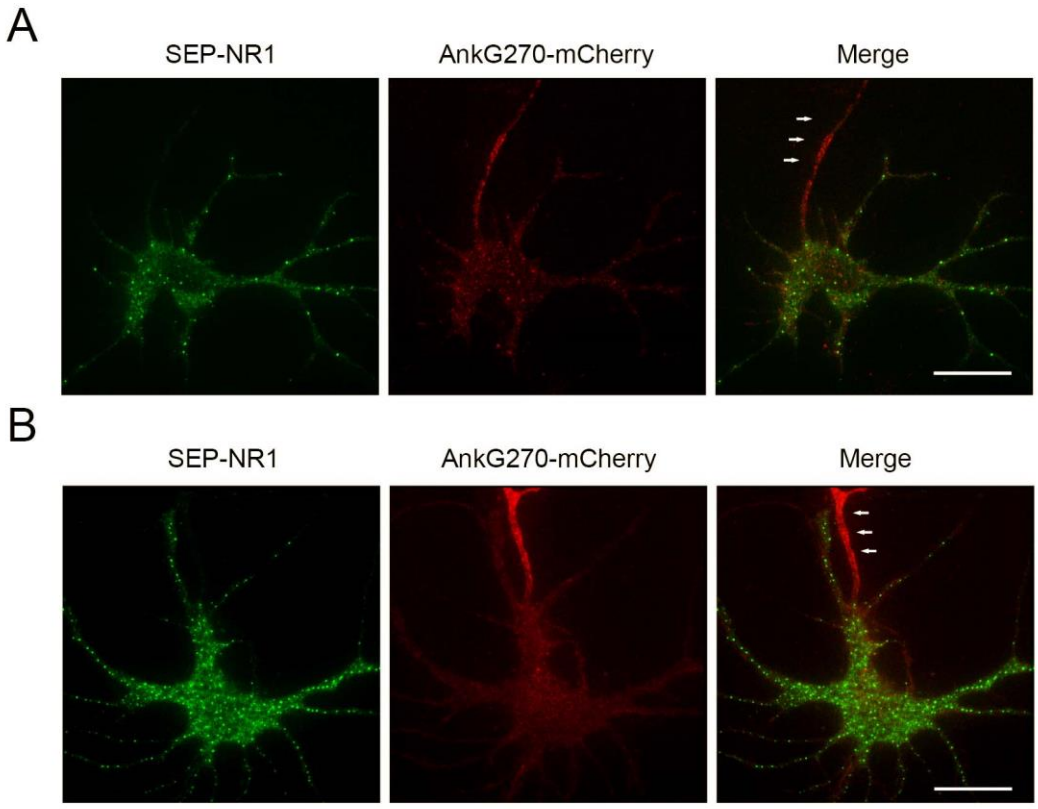

Fig. S8. Identification of distinct functional compartments in live hippocampal neurons

Selective enrichment of AnkG270-mCherry in axon initial segments (highlighted by white arrows) in live DIV 6 (*A*) and DIV 12 (*B*) hippocampal neurons. In contrast, membrane bound NMDA receptors labeled by Superecliptic pHluorin (SEP)-NR1 were selectively localized to dendrites. For the experiment, primary hippocampal neurons were co-transfected with the AnkG270-mCherry and SEP-NR1 expression plasmids at DIV 0 and then were cultured to the indicated stages before live HILO imaging. Scale bar: 10 µm

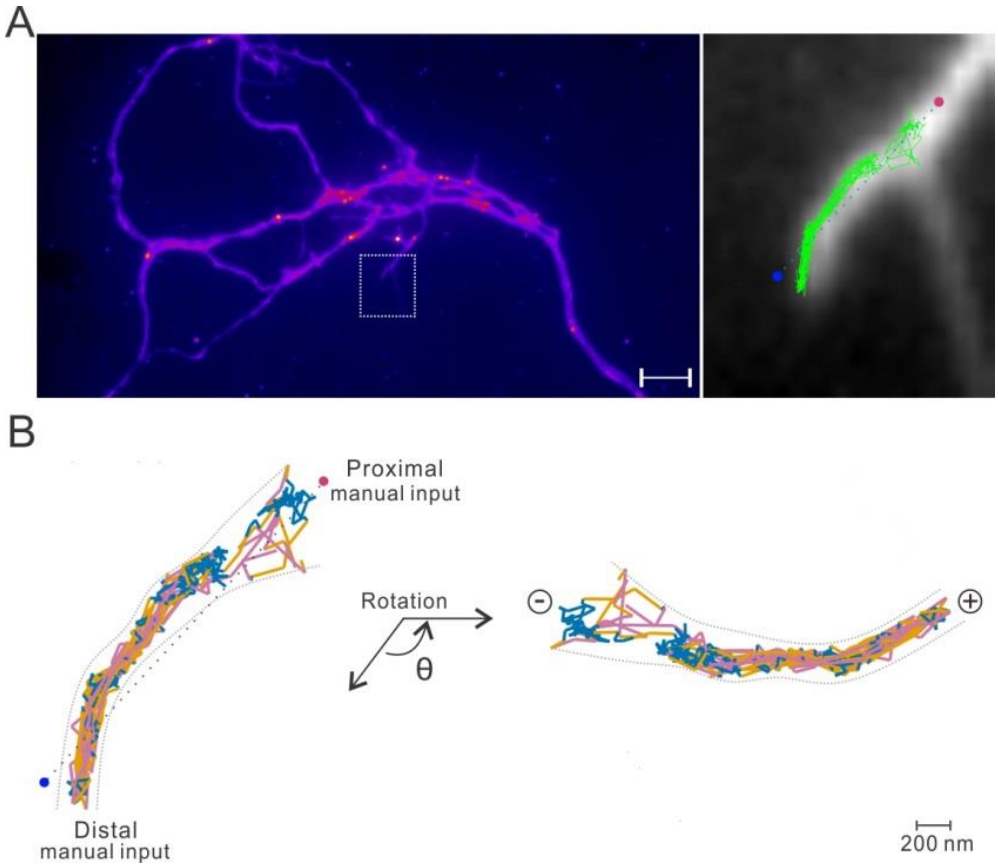

Fig. S9. Alignment and normalization of anterograde and retrograde transport direction.

(*A*) Left panel: an image showing complex neurite paths in the axon. Right panel, the zoom-in view of the rectangle region indicated in the left panel. The trajectory (Green) is overlaid with the image. Manually selected proximal and distal points of the neurite path are shown as the red dot and the blue dot, respectively. Scale bar: 5 μm

(*B*) The trajectory is rotated by the angle (ɵ) between the vector (from the proximal to the distal point) and the *x* axis, with the anterograde transport pointing to the '+' direction.

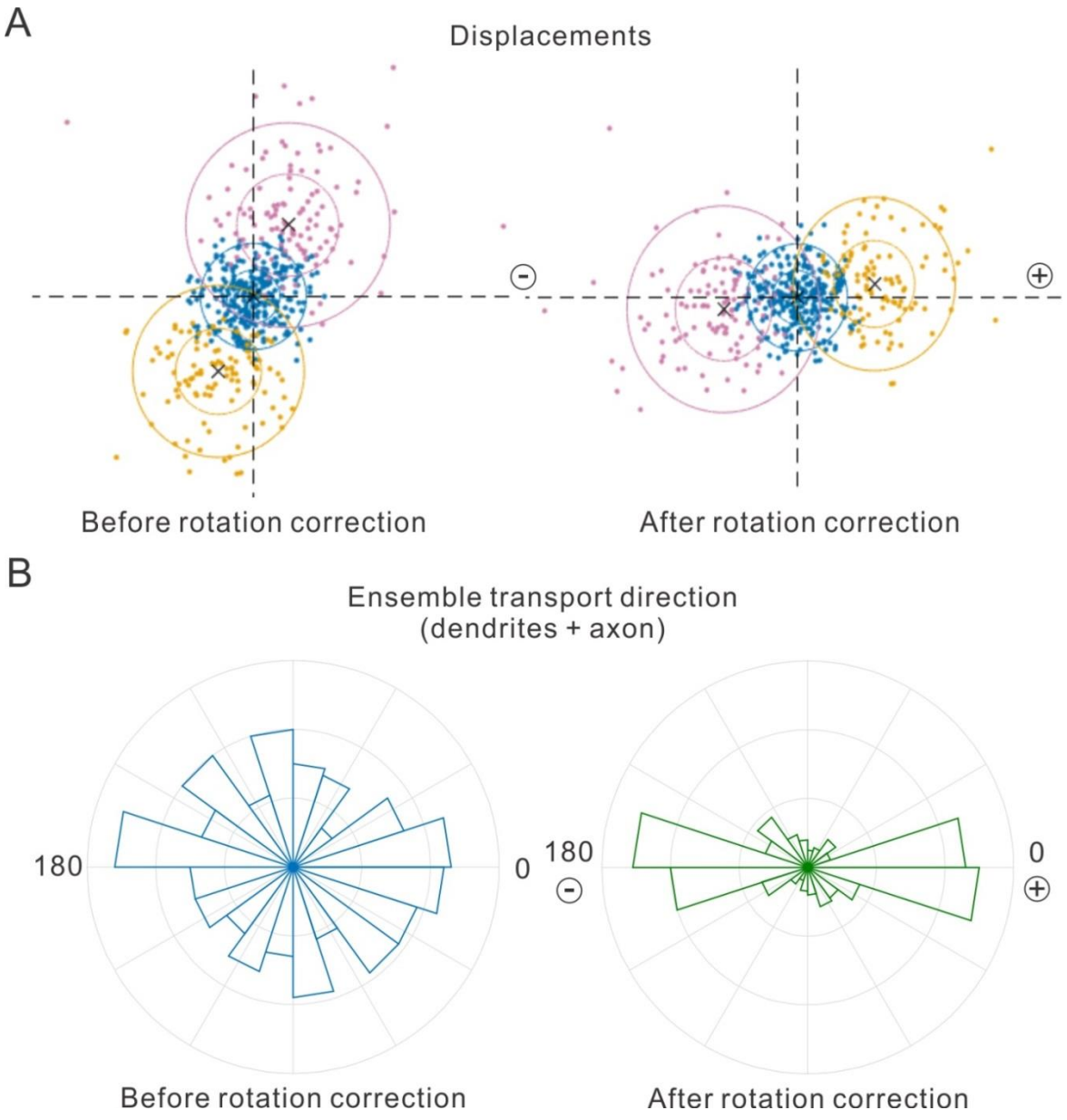

Fig. S10. Statistics after the rotation correction

(*A*) The displacements in the trajectory shown in **Fig. S9** before (left panel) and after (right panel) the rotation correction.

(*B*) Ensemble active transport directions before (left panel) and after (right panel) the rotation correction for all trajectories. After the rotation correction step, transport events were bifurcated to either anterograde (+) or retrograde (-) transport processes.

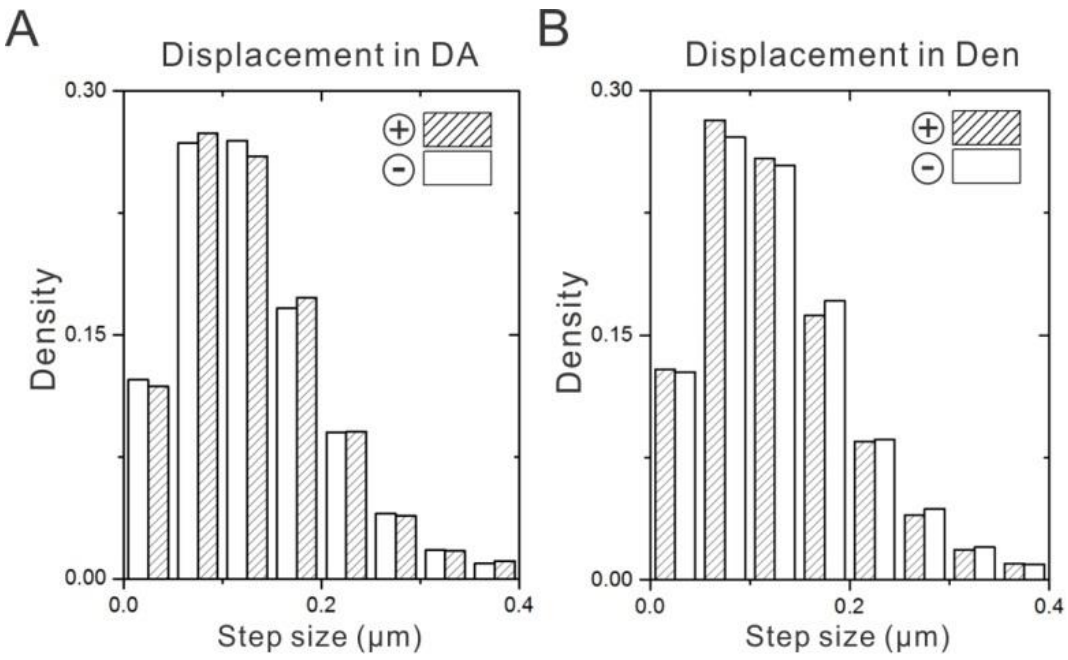

C

	D(μm²/s)	%(D)	τ^D(ms)
Soma	0.084 ± 0.04	75%	211 ± 82
AIS	0.063 ± 0.03	58%	110 ± 44
DA	0.090 ± 0.06	65%	142 ± 59
Den	0.076 ± 0.05	51%	153 ± 64

Fig. S11. Compartment-specific SVP/SV dynamics.

(*A*) The step size distribution for anterograde (+) and retrograde (-) transport processes in the distal axon (DA).

(*B*) The step size distribution for anterograde (+) and retrograde (-) transport processes in the dendrites (Den.).

(*C*) Statistic summary for the diffusion state in different neuronal compartments. D, diffusion coefficient; %, time fraction; τ, state lifetime; See *Supplementary Methods* for more calculation details. D and τ^D are shown in mean ± SD. For τ^D in AIS versus in other regions: *p*-value < 6.7e-7, F = 75.34, df = 796.

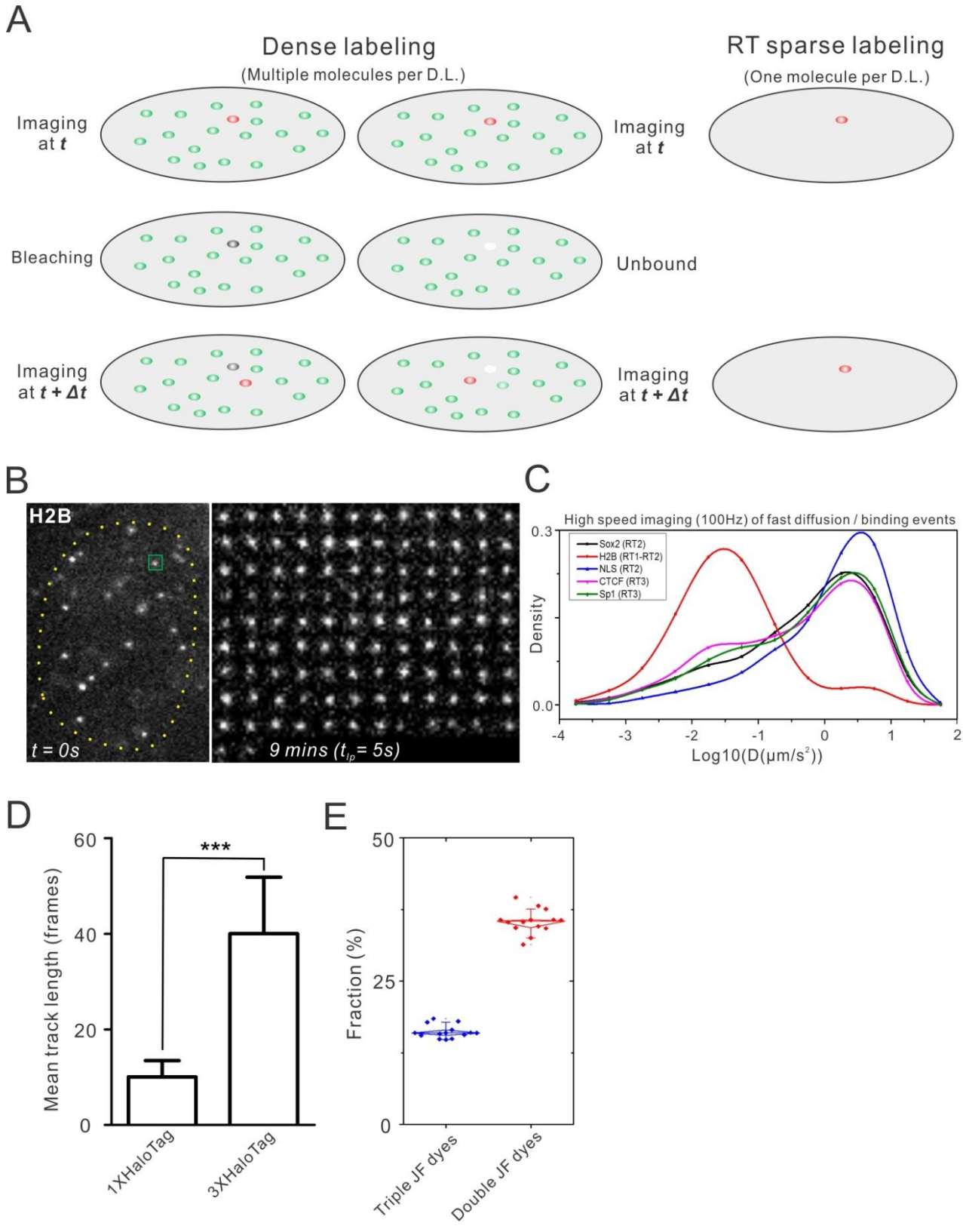
A
Dense labeling
(Multiple molecules per D.L.)
RT sparse labeling
(One molecule per D.L.)
Imaging at t
Imaging at t
Bleaching
Unbound
Imaging at t + Δt
Imaging at t + Δt
B
H2B
t = 0s
9 mins (tlp = 5s)
C
High speed imaging (100Hz) of fast diffusion / binding events
Sox2 (RT2)
H2B (RT1-RT2)
NLS (RT2)
CTCF (RT3)
Sp1 (RT3)
Density
0.3
0.0
-4
-3
-2
-1
0
1
2
Log10(D(μm/s²))
D
Mean track length (frames)
60
40
20
0
***
1XHaloTag
3XHaloTag
E
Fraction (%)
50
25
0
Triple JF dyes
Double JF dyes

Fig. S12. Long-term imaging of TF dynamics in live cells

(*A*) Left, long lapse times could introduce tracking artifacts in densely labeled samples. Specifically, if one molecule is bleaching or unbound after one imaging frame, due to the dense labeling, the probability is high for another molecule to be activated or diffuse in during the dark time, contaminating the tracking results.

Right, in average, only one labeled molecule exists in one diffraction limit in the sparse labeling condition. Thus, the tracking problem mentioned above could be avoided.

(*B*) With a 5 *sec* lapse time (t_{lp}), one representative H2B chromatin binding event can be directly observed for ~9 mins. The first frame image of the whole nucleus is shown in the left panel. The temporal file of one binding event (highlighted by the green square) is shown in the montage image (right). Also see **Movie S8**.

(*C*) Density histogram of log10 (Diffusion coefficient) for all trajectories captured by 100 Hz fast 2D single-molecule imaging. As expected, fusion of transcription factor to 3XHaloTag leads to more slow diffusion events in live cells, in comparison to 3XHaloTag-NLS.

(*D*) Averaged track length of 1XHaloTag – H2B (dSTORM) and 3XHaloTag-H2B (the RT strategy) using continuous acquisition (2 Hz; *p*-value < 0.0001, t = 7.729, df = 18, n = 10 cells for each condition). See *Supplementary Methods* for experimental conditions. ***, *p*-value < 0.001

(*E*) The fractions of 3XHaloTag labeled with triple and double JF dyes estimated by using **Eqn. S1 - S7.**

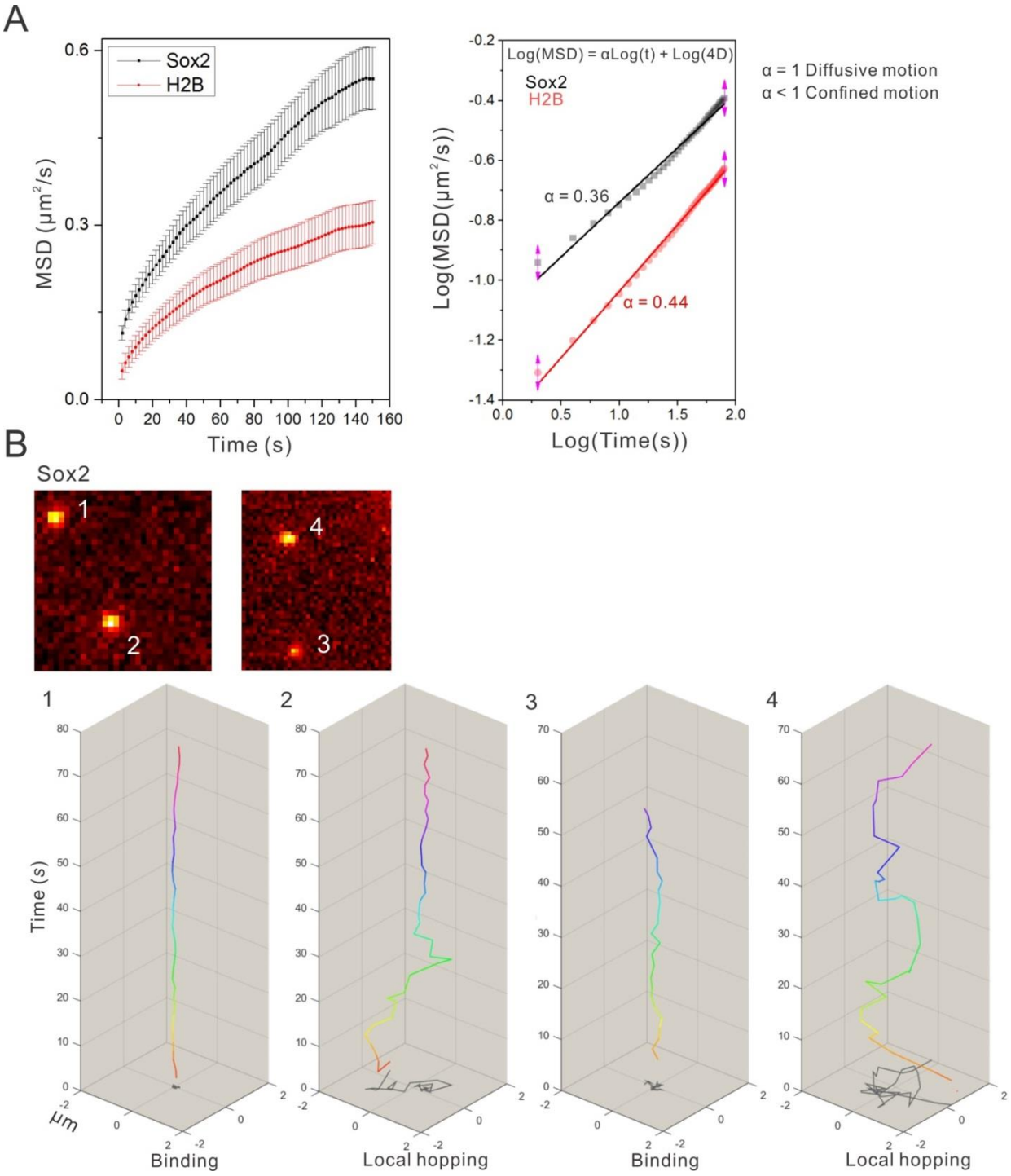

Fig. S13. Sox2 hops locally in the nucleus

(*A*) Left, MSD plot shows that Sox2 molecules are more dynamic than H2B at the slow diffusion state in ES cells. The lapse time is 2 *sec* (**Fig. 4*A***). (Number of Trajectories: 1317 (H2B); 2118 (Sox2)).

Right, Log-log linear regression to calculate the motion-type indicator (α) for Sox2 slow diffusion events. See **Eqn. S12** and **S13** for calculation details.

(*B*) Two Sox2 molecules in the same fields of view (1 and 2, 3 and 4) have different diffusion characteristics (stable binding and local hopping), suggesting that the local hopping behavior observed was not caused by cell movement or imaging platform drift. See **Movie S9** for the raw imaging data and track overlay.

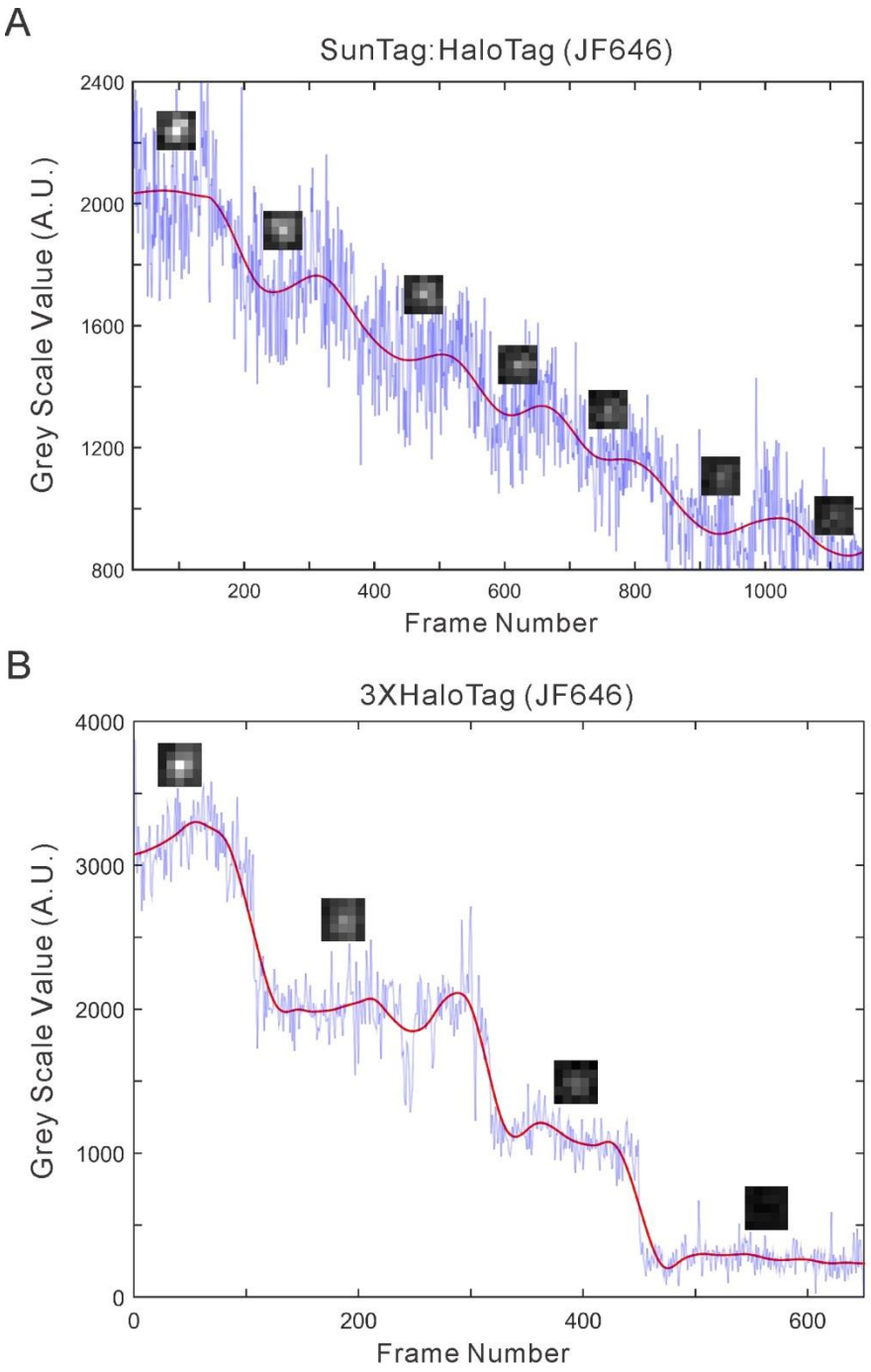

Fig. S14. Step-wise photobleaching of SunTag-labeled synaptic vesicles and 3XHaloTag-H2B

(*A*) The intensity change over time captured by continuous imaging of SunTag (HaloTag, JF646)-labeled single synaptic vesicle with ~20 W/cm^2 647 laser. After analysis, 6 steps of

fluorescent drop could be observed. The insets show the single molecule images corresponding to each event after fluorescent drop. Acquisition rate: 10 Hz

(*B*) The intensity change over time captured by continuous imaging of single 3XHaloTag (JF646)-H2B molecule with ~100 W/cm^2 647 laser. After analysis, 3 steps of fluorescent drop could be observed. The insets show the single molecule images corresponding to each event after fluorescent drop. Acquisition rate: 10 Hz

SUPPLEMENTARY TABLE

Table S1: Localization and Tracking Parameters for the MTT program

Localization Error	1E-06	
Deflation loops	3	
Blinking (frames)	1	
Maximum number competitors	3	
Maximum Diffusion Coefficient ($\mu m^2/s$)	5	For SVP/SV HMM-Bayes analysis (50 Hz)
Maximum Diffusion Coefficient ($\mu m^2/s$)	0.5	For SVP/SV MSD analysis (50 Hz)
Maximum Diffusion Coefficient ($\mu m^2/s$)	0.1	For TF slow acquisition (2 Hz)
Maximum Diffusion Coefficient ($\mu m^2/s$)	5	For TF fast tracking (100 Hz)

SUPPLEMENTARY METHODS

Cell Culture

Mouse D3 (ATCC) ES cells were maintained on 0.1% gelatin coated plates in the absence of feeder cells. The ES cell medium was prepared by supplementing knockout DMEM (Invitrogen) with 15% FBS, 1 mM glutamax, 0.1 mM nonessential amino acids, 1 mM sodium pyruvate, 0.1 mM 2-mercaptoethanol and 1000 units of LIF (Millipore). NIH/3T3 cells and U2OS cells were maintained in DMEM medium (Corning, without phenol-red) supplemented with 10% FBS, 1 mM glutamax. SH-SY5Y cells were cultured in DMEM/F12 medium (Gibco, without phenol-red) supplemented with 10% FBS.

Electroporation was used to transfect ES cells. Specifically, the Amaxa 4D-Nucleofector System and the kit for Mouse Embryonic Stem Cells (Lonza) were used according to manufacturer's suggestions. We used Lipofectamine 3000 reagent (Invitrogen) for transfecting NIH/3T3 cells, U2OS cells and SH-SY5Y cells. For generating stable cell lines, cells were co-transfected with Piggybac transposon vector (neomycin-resistant) and a helper plasmid that encodes Piggybac transposase (Supper Piggybac Transposase, System Biosciences). Two days post-transfection, the cells were subjected to G418 (Thermo Fisher Scientific) selection.

Primary Culture of Hippocampal Neurons

We prepared dissociated hippocampal neurons from P0 to 1 Sprague-Dawley rat pups. Briefly, the hippocampi were dissected out and digested with papain (Worthington Biochemical). After digestion, the tissues were gently triturated and filtered with the cell strainer. The cell density was counted. ~2.5×10^5 cells were transfected with indicated constructs by using P3 Primary Cell 4D-Nucleofector X kit (Lonza). After transfection, neurons were plated onto poly-D-lysine

(PDL, Sigma)-coated coverslips and maintained in NbActiv4 medium (BrainBits) at 37 °C for indicated days before imaging.

Plasmids and Molecular Cloning

H2B, Sox2, and Sp1 cDNA were amplified from constructs used in our previous studies (2, 3). CTCF cDNA was amplified from ES cell cDNA libraries. Synaptophysin cDNA and 24xGCN4 (SunTag) cDNA were obtained from Addgene (Plasmid #51509 and Plasmid #72229). The scFv-GCN4-sfGFP-NLS, ankG-mCherry, and SEP-NR1 constructs were obtained from Addgene (Plasmid #60906, Plasmid #42566, and Plasmid #23999). The DNA fragment of 3XHaloTag with M to L substitutions was synthesized by Integrated DNA Technologies. The cDNA fragments were cloned into Piggybac transposon vector (PB533A-2, System Biosciences) or modified Piggybac transposon vector with EF1, SV40, human PGK or human synapsin 1 promoter. HaloTag (Promega) was used to replace the sfGFP region to get scFv-GCN4-halo-NLS construct. The plasmids used for fish microinjection were made using the Tol2-Gateway system and the pDEST vector was used as the destination construct.

Real time PCR

Total RNA was extracted with Trizol Reagent and reverse-transcribed by SuperScript III Reverse Transcriptase with oligo-dT primer (Thermo Fisher Scientific). cDNA corresponding to 5 ng of total RNA was used in each SYBR Select Master Mix (Thermo Fisher Scientific) reaction. Reactions were performed in duplicates and the results were collected on a CFX96 Touch Real Time PCR Detection System (Bio-Rad).

The PCR primers for H2B-mEOS4b-HA construct are:

Forward: 5-AATGTATGTGCGTGATGGAGTG-3

Reverse: 5-TATGGGTAACCTGAACCTGATC-3

The primers for human GAPDH are:

Forward: 5- AACGGATTTGGTCGTATTGGGC-3

Reverse: 5- CCTGGAAGATGGTGATGGGAT-3

Western Blot

Whole cell extracts from U2OS cells were isolated using RIPA buffer that contained Complete Protease Inhibitor Cocktail (Roche). Protein concentrations were measured using Bio-Rad Protein Assay against BSA standards. Protein from each sample was resolved by SDS-PAGE. Primary antibodies used: HA tag (ab9134, Abcam, 1:500) and beta-tubulin (#2128, Cell Signaling Technology, 1:1000). HRP conjugated secondary antibodies (Pierce) were used at a dilution of 1:2000. LumiGLO chemiluminescent substrate (Cell Signaling Technology) was used for HRP detection and light emission was captured by films.

Immunofluorescence Staining

Cells were first fixed with 4% paraformaldehyde, permeabilized and blocked with 10% goat serum, 1% BSA, and 0.25% Triton in PBS. Samples were stained with synaptophysin (ab8049, Abcam, 1:500) or synapsin 1 (AB1543P, Millipore, 1:5000) primary antibodies in PBS containing 10% goat serum, 1% BSA, and 0.1% Triton. Secondary antibodies: DyLight 488 conjugated secondary antibodies (Jackson ImmunoResearch, 1:400).

Immuno-EM Experiment

Primary hippocampal neurons were grown on PDL-coated 8-well chamber slide (Thermo Fisher Scientific) for 10 ~ 14 days. Pre-embedding immunogold labeling was performed on the wells as previously reported (4). Briefly, Neuronal cultures were fixed with 4% paraformaldehyde/0.05% glutaraldehyde in sodium cacodylate buffer (0.1 M, pH 7.2). After washing with cacodylate buffer and PBS, samples were blocked with 50 mM glycine in PBS and permeabilized in PBS containing 5% normal goat serum and 0.1% saponin. Then they were incubated with anti-GFP antibody (A-11122, Thermo Fisher Scientific, 1:200) first and Nanogold-Fab' fragment of goat anti-rabbit IgG (Nanoprobes; 1:150) later. After silver enhancement (HQ kit, Nanoprobes) for 6 minutes, the samples were treated with 0.5% osmium tetroxide in phosphate buffer, dehydrated in ethanol and finally embedded in Eponate 12 resin (Ted Pella, Inc) for ultrathin sectioning. Ultrathin sections were contrasted with aqueous uranyl acetate and lead citrate and imaged on a Tecnai Spirit electron microscope (FEI, Hillsboro, OR) using an Ultrascan 4000 (Gatan, Inc) digital camera.

Microinjection and imaging of *zebrafish*

Using a *zebrafish* gal4-vp16 driver line under the control of the pan-neuronal Huc promoter, embryos were co-injected at the 1 or 2-cell stage with plasmid DNA of UAS (5X)-syp-RT1-24xGCN4 at 25 ng/µl and 8 ng/µl for UAS (10X)-scFv-GCN4-sfGFP-NLS along with 25 ng/µl Tol2 mRNA. Fish were examined 48 ~ 60 hours later for GFP fluorescence and positive ones were picked to do the HILO imaging on a Nikon Eclipse TiE Motorized Inverted microscope equipped with a 100X Oil-immersion Objective lens (Nikon, N.A. = 1.49).

Cell Labeling Strategy and Preparation for Imaging

Transfected hippocampal neurons were plated onto an ultra-clean cover glass pre-coated with PDL and cultured for indicated days (DIV 6 or DIV 12). For live imaging, culture medium was replaced with Tyrode's solution (140 mM NaCl, 5 mM KCl, 3 mM $CaCl_2$, 1 mM $MgCl_2$, 10 mM HEPES, 10 mM glucose, pH 7.35).

Stable ES cell lines were plated onto an ultra-clean cover glass pre-coated with IMatrix-511 (Clontech). ES cell imaging experiments were performed in the ES cell imaging medium, which was prepared by supplementing FluoroBrite medium (Invitrogen) with 10% FBS, 1 mM glutamax, 0.1 mM nonessential amino acids, 1 mM sodium pyruvate, 10 mM HEPES (pH 7.2 ~ 7.5), 0.1 mM 2-mercaptoethanol and 1000 units of LIF (Millipore).

Transfected NIH3T3 and U2OS cells were plated onto an ultra-clean cover glass without coating. The NIH3T3 and U2OS imaging medium was prepared by supplementing FluoroBrite medium (Invitrogen) with 10% FBS, 1 mM glutamax, 0.1 mM nonessential amino acids and 1 mM sodium pyruvate.

For the saturated labeling of SunTag (24XHaloTag) or 3XHaloTag, cells were incubated with JF646-HTL or JF549-HTL with final concentration of 500~1000 nM for 30 mins. HTL stands for HaloTag Ligand. Chemical structures and synthesis procedures of JF549-HTL and JF646-HTL were described previously (5).

To image single molecules without using the sparse labeling strategy, we first tested the optimal HaloTag-JF549 and HaloTag-JF647 labeling concentrations. Several concentrations of JF549-HTL and JF646-HTL (0.5 nM, 1 nM, 2 nM and 5 nM) were used to treat cells for 15 mins and then cells were washed with imaging medium for 3 times. The cover glasses were then transferred to live-cell culturing metal holders and mounted onto the microscope one by one. Proper HaloTag-JF549 or HaloTag-JF646 labeling concentrations were determined by the

criterion that single-molecules can be easily detected after no or a minimal 2 ~ 5 *sec* pre-bleaching. After fixing the labeling concentration for each cell line, we then proceeded to perform the 2D single-molecule imaging experiments.

PALM Imaging to Estimate RT Efficiency

Live-cell PALM imaging experiments were used to estimate the H2B-mEOS4b labeling densities (**Fig. 1** ***B***, ***C***, ***D*** and ***E*** and **Fig. S3*A*** and **Movie S1**). Specifically, imaging was performed on a Nikon Eclipse TiE Motorized Inverted microscope equipped with a 100X Oil-immersion Objective lens (Nikon, N.A. = 1.49), four laser lines (405/488/561/642), an automatic TIRF illuminator, a perfect focusing system, a tri-cam splitter, three EMCCDs (iXon Ultra 897, Andor) and Tokai Hit environmental control (humidity, 37 °C, 5% CO_2). Proper emission filters (Semrock) were switched in front of the cameras for GFP, JF549 or JF646 emission and a band mirror (405/488/561/633; BrightLine quad-band bandpass filter, Semrock) was used to reflect the laser into the objective. For sparse single-molecule imaging, mEOS4b moiety was stochastically converted from 'Green' to 'Red' state with low-dose 405 nm illumination (5 ~ 10 W/cm^2). Then, single molecules were imaged at 50 Hz using a 561 nm laser with the excitation intensity of ~1000 W/cm^2. 5000 frames were collected for each cell. For each RT condition, data from 10 ~ 20 cells were collected.

Imaging SVP Dynamics

SVP particles were imaged using TIRF with our Nikon Eclipse TiE set-up described above. For tracking SunTag-GFP labeled SVPs, we used a 488 nm laser with the excitation intensity of ~100 W/cm^2. For tracking SunTag-HaloTag-JF549/646 labeled SVPs, we used a laser with the

excitation intensity of ~50 W/cm^2. For imaging HaloTag-JF549 labeled SVPs, we used a 561 nm laser with the excitation intensity of ~1000 W/cm^2. An acquisition time of 20 ms was applied for both conditions. For step-wise photobleaching of SunTag-HaloTag-JF646 labeled SVPs, we used 647 laser with the excitation intensity of ~20 W/cm^2 and an acquisition time of 100 ms.

Single-molecule Imaging of Long-lived Chromatin Binding Events

For imaging immobile TF or H2B binding events in live nuclei, we used the same Nikon Eclipse TiE set-up described above. The TIRF illuminator was adjusted to deliver a highly inclined laser beam to the cover glass with the incident angle smaller than the critical angle. Thus, the laser beam is laminated to form a light-sheet (~3 μm) above the cover glass. The oblique illumination (HILO) has much less out-of-focus excitation, compared with the regular Epi-illumination. TFs labeled with 3XHaloTag-JF549 were imaged using a 561 nm laser with the excitation intensity of ~50 W/cm^2. To specifically probe long-lived binding events, we used 500 ms imaging acquisition time to blend fluorescence signals from fast diffusing molecules into the imaging background by motion blur (3, 6). Because we only measure stable binding events at the focal plane by motion blur, fast 3D motion should not affect the measurements. We also introduced long dark times (τ_D) between imaging frames to minimize photobleaching as previously described (7). The dark times vary from 0 *sec* to 4.5 *sec*. To minimize drift during imaging, we performed imaging in an ultra-clear room with the precise temperature control system. The environment control chamber for cell culturing was fully thermo- equilibrated and any devices that introduce mechanical vibrations are separated from the air table where the microscope body resides. We calibrated our imaging system with beads to confirm minimal drift during imaging (*xy* drift < 100 nm per hour). For step-wise photobleaching of 3XHaloTag-JF647 labeled H2B, we used 647 laser with the excitation intensity of ~100 W/cm^2 and an acquisition time of 100 ms.

Single-Molecule Localization, Tracking and Diffusion Analysis

For 2D single-molecule localization and tracking, the spot localization (x,y) was obtained through 2D Gaussian fitting based on MTT algorithms (8). The localization and tracking parameters in SPT experiments are listed in the **Table S1**. The resulting tracks were inspected manually. The RT efficiencies (in %, **Fig. 1** ***C***, ***D*** and ***E*** and **Fig. S3*A***) were calculated by normalizing single-cell localization density from each RT condition to the average density in the no RT control. Diffusion coefficients (**Fig. 4*E*** and **Fig. S5*E***, **12*C*** and **13*A***) were calculated from tracks with at least 5 consecutive frames by the MSDanalyzer (9) with a minimal fitting R^2 of 0.8.

HMM-Bayes Analysis of SVP Dynamics

The diffusion and transport states of individual SVP trajectories were analyzed by HMM-Bayes program (10) with default parameters. Specifically, maximal 3 states can be inferred from one trajectory. There are possibilities for one or two states as well (*e.g.* **Fig. 2** ***C*** and ***D***). In the HMM-Bayes analysis, the transport process is modeled as directed motion (V) with Brownian diffusion (D) according to the classical equation, $< r^2 >= 4D\Delta t + (V\Delta t)^2$ (11). The program categorizes each step in the trajectory to either diffusion or transport processes and calculates diffusion coefficient as well as transport velocity. To separate anterograde and retrograde transport processes, we rotate the trajectory and align the neurite along the x axis with the anterograde transport point to '+' direction. Specifically, for each trajectory, we manually defined one proximal and one distal point along the neurite and then the angle ɵ between the vector (from the proximal to the distal point) and the '+' direction of *x* axis was calculate by *atan2 ()* function in Matlab 2015a. Subsequently, the trajectory was rotated by - ɵ. After the rotation correction, the transport processes bifurcated to anterograde and retrograde direction (**Fig. S9**

and **S10**). For each functional compartment (soma, dendrites, distal axon and axon initial segment) in the neuron, the average diffusion coefficients, transport velocities and life-time of different states (**Fig. 2*D*** and **3 *C***, ***D*** and ***E*** and **Fig. S11**) were calculated. In total, data from 20 ~ 30 cells were analyzed for each compartment. The standard deviation reflects cell-to-cell variations.

TF Residence Time Analysis

To map stable bound sites in the slow acquisition (500 ms) and time lapse condition, 0.1 $\mu m^2/s$ was set as maximum diffusion coefficient (D_{max}) for the tracking. The D_{max} works as a limit constraining the maximum distance (R_{max}) between two frames for a particle random diffusing during reconnection. Only molecules localized within R_{max} for at least two consecutive frames will be considered as bound molecules. The duration of individual track (dwell time) was directly calculated based on the track length.

The relationship between photo-bleaching and dissociation can be described by the following diagram and differential equations, where n_0 is the number of 3XHaloTag with 3 bright dye molecules at a given time; n_1 is the number of 3XHaloTag with 2 bright JF dye molecules at a given time; n_2 is the number of 3XHaloTag with 1 bright JF dye molecules at a given time; k_{off} is the TF dissociation rate; k_b is the photo-bleaching rate.

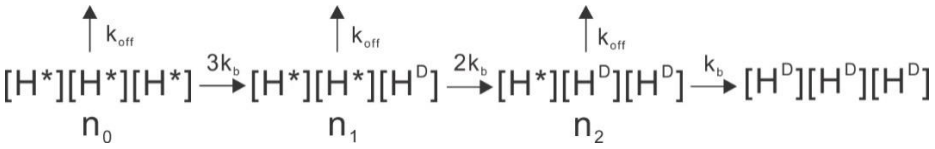

H^*, HaloTag with a bright dye molecule. H^D, HaloTag with a bleached dye molecule.

$$\frac{dn_0}{dt} = -(3k_b + k_{off})n_0 \qquad \textbf{Eqn. S1}$$

$$\frac{dn_1}{dt} = 3k_b n_0 - 2k_b n_1 - k_{off} n_1 \qquad \textbf{Eqn. S2}$$

$$\frac{dn_2}{dt} = 2k_b n_1 - k_b n_2 - k_{off} n_2 \qquad \textbf{Eqn. S3}$$

Here, we define N_T as the number of 3XHaloTag labeled with JF dye molecules before imaging; α as the percentage (N_0/N_T) of triple-labeled molecules before imaging and β as the percentage (N_1/N_T) of double-labeled molecules before imaging.

By solving the differential equations **1 - 3**, we can establish the relationship between the number of observable single molecules ($N_{bright}(t)$), k_{off}, k_b, α and β.

$$N_{bright}(t) = n_0 + n_1 + n_2 = N_T\left[(1 + 2\alpha + \beta)e^{-(k_{off}+k_b)t} + \alpha e^{-(k_{off}+3k_b)t} - (3\alpha + \beta)3e^{-(k_{off}+2k_b)t}\right] \quad \textbf{Eqn. S4}$$

The time lapse photo-bleaching rate is equal to $k_b \frac{\tau_{int}}{\tau_{lp}}$, τ_{lp} is the lapse time, τ_{int} is camera acquisition time. Thus **Eqn. S4** can be transformed to

$$N_{bright}(t) = N_0\left[(1 + 2\alpha + \beta)e^{-\left(k_{off}+k_b\frac{\tau_{int}}{\tau_{lp}}\right)t} + \alpha e^{-\left(k_{off}+3k_b\frac{\tau_{int}}{\tau_{lp}}\right)t} - (3\alpha + \beta)e^{-\left(k_{off}+2k_b\frac{\tau_{int}}{\tau_{lp}}\right)t}\right] \quad \textbf{Eqn. S5}$$

Here we further assign

$$k_m = k_{off} + k_b \frac{\tau_{int}}{\tau_{lp}} \qquad \textbf{Eqn. S6}$$

And, **Eqn. S5** can be rearranged to,

$$\frac{N_{bright}(t)}{N_0} = (1 + 2\alpha + \beta)e^{-k_m t} + \alpha e^{-\left(k_m+2k_b\frac{\tau_{int}}{\tau_{lp}}\right)t} - (3\alpha + \beta)e^{-\left(k_m+k_b\frac{\tau_{int}}{\tau_{lp}}\right)t} \quad \textbf{Eqn. S7}$$

Fitting 1-CDF curve with **Eqn. S7** yields k_m, α and β for different time lapse conditions. The fitting was performed using *lsqnonlin* function in Matlab 2015.

Eqn. S6 can be transformed into **Eqn. S8**

$$k_m\tau_{lp} = k_{off}\tau_{lp} + k_b\tau_{int} \qquad \textbf{Eqn. S8}$$

Therefore, the dissociation rate (k_{off}) can be derived through linear fitting $k_m\tau_{lp}$ as a function of τ_{lp} similar to the previous publication (7).

Jumping Angle Analysis

A sliding window of 3 points was applied to each track. The angle between the vectors of the first two and the last two points was calculated by the *acos()* function in the Matlab 2015a. Individual angles were pooled and binned accordingly for the angular Rose histogram (**Fig. 2*D*** and **Fig. S10*B***). The minimal jumping distance between two points is set as 40 nm to ensure that the angle measurement is not significantly affected by the localization uncertainty.

Labeling Density Simulation and Motion-type Detection

For a 10 μm × 10 μm square area (**Fig. S1*A***) or for a 50 μm linear neurite (**Fig. S5*D***), the (x, y) positions for *N* single molecules were first randomly generated based on a uniform distribution in 2D or 1D. The photon counts contributed from each molecule to individual pixels (160 nm × 160 nm) were calculated based on the PSF estimator below.

$$I_i(x,y) = \left(A_0 e^{\frac{-(x-x_0)^2}{2\sigma_{xy}^2}} e^{\frac{-(y-y_0)^2}{2\sigma_{xy}^2}}\right)_{PSF} \qquad \textbf{Eqn. S9}$$

Specifically, A_0 is the signal amplitude; σ is the Standard Deviation (S.D.: ~250 nm) of the Gaussian fit in the indicated direction, in our case S.D. of the x, y direction is the same.

To form the image, we first introduced random white noises (B_{xy}) in the area with pixel intensities ranging from 0 ~ $A_0/5$ (Signal-to-Background Ratio > 5). Then, the pixel intensity

$I(x,y)$ was calculated by iteratively summing the photon counts contributed from each molecule above the background value, according to equation below:

$$I(x,y) = \sum_1^N I_i\,(x,y) + B_{xy} \qquad \textbf{Eqn. S10}$$

In **Fig. S1**, we used the Einstein's Brownian diffusion equation to calculate the expected jumping distance between frames.

$$< r >= 2\sqrt{D\Delta t} \qquad \textbf{Eqn. S11}$$

Note that when the motion is confined, the MSD curve is situated below its tangent at Δt = 0. Therefore, if we model coarsely the MSD curve by a power law according to 2D diffusion models (11).

$$< r^2 >= 4D\Delta t^{\alpha} \qquad \textbf{Eqn. S12}$$

We should get α = 1 for purely diffusive motion, and α < 1 for confined motion. So we could determine from our experimental data a power law coefficient. This is best made in a log-log fashion (**Fig. S13*A***), for which power laws turn to linear laws:

$$Log(\mathrm{MSD} < r^2 >) = \alpha Log(\Delta t) + Log(4D) \qquad \textbf{Eqn. S13}$$

Numerical Simulation of Protein Copy Number in the Cell

Because the number of reacting DNA molecules is small, random molecular fluctuations become significant and discrete, Gillespie stochastic simulation algorithm (SSA) approach (12) is applied in this case. Such a system can be modeled as a continuous-time Markov process, whose probability distribution obeys what is called a chemical "master equation". We used the Gillespie's Direct Method for the simulation. We first provided a model consisting of a matrix of reaction rates, a function that computes reaction propensities (probability/unit time), an initial

state vector, and initial/final times. The SSA functions return the sequence of event times and protein/RNA species amounts.

The master gene expression model is defined by the following reaction and parameters:

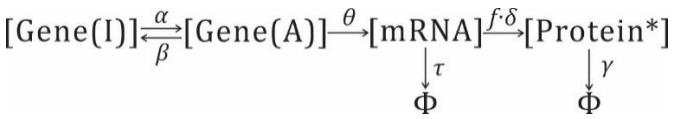

α, Gene Activation Rate

β, Gene Inactivation Rate

θ, mRNA Production Rate

δ, Translation Rate

f, Read-Through Rate

δ, Translation Rate

α, mRNA degradation Rate

γ, Protein degradation Rates

$*$, Labeled Protein

According to previous modeling calculation (13), the mean copy number of labeled proteins is given by:

$$< Protein^{*} >= f\frac{\delta}{\gamma}\frac{\theta}{\tau}\frac{\alpha}{\alpha+\beta} \qquad \textbf{Eqn. S14}$$

In the simulation, we kept mRNA Production Rate (θ), mRNA degradation Rate (α), Translation Rate (δ) and Protein degradation Rate (γ) constant. We used a RT Rate (f) of 0.5%, similar to

the efficiency of RT3. We adjusted the promoter strength by tuning the fraction of the promoter on time (%), which is equal to $\alpha/(\alpha+\beta)$. For reliable single-molecule tracking, we maintained the average protein copy number in the simulation as ~40 copies per cell. Here we defined the protein noise (η) as the standard deviation divided by the mean.

Statistics

Comparisons between two groups were performed with Student's *t*-test. Comparisons among multiple groups were performed with one-way or two-way ANOVA (**Fig. S11*C*** and **Fig 1 *D*** and ***E***). Error bars in all figures represent SD, except the box charts. Differences were considered to reach statistical significance when $p < 0.05$.

SUPPLEMENTARY REFERENCES

1. Tokunaga M, Imamoto N, & Sakata-Sogawa K (2008) Highly inclined thin illumination enables clear single-molecule imaging in cells. *Nature methods* 5(2):159-161.
2. Li L*, et al.* (2016) Real-time imaging of Huntingtin aggregates diverting target search and gene transcription. *Elife* 5:e17056.
3. Chen J*, et al.* (2014) Single-molecule dynamics of enhanceosome assembly in embryonic stem cells. *Cell* 156(6):1274-1285.
4. Tao-Cheng JH (2006) Activity-related redistribution of presynaptic proteins at the active zone. *Neuroscience* 141(3):1217-1224.
5. Grimm JB*, et al.* (2015) A general method to improve fluorophores for live-cell and single-molecule microscopy. *Nature methods* 12(3):244-250.
6. Swinstead EE*, et al.* (2016) Steroid Receptors Reprogram FoxA1 Occupancy through Dynamic Chromatin Transitions. *Cell* 165(3):593-605.
7. Gebhardt JC*, et al.* (2013) Single-molecule imaging of transcription factor binding to DNA in live mammalian cells. *Nature methods* 10(5):421-426.
8. Serge A, Bertaux N, Rigneault H, & Marguet D (2008) Dynamic multiple-target tracing to probe spatiotemporal cartography of cell membranes. *Nature methods* 5(8):687-694.
9. Tarantino N*, et al.* (2014) TNF and IL-1 exhibit distinct ubiquitin requirements for inducing NEMO-IKK supramolecular structures. *The Journal of cell biology* 204(2):231-245.
10. Monnier N*, et al.* (2015) Inferring transient particle transport dynamics in live cells. *Nature methods* 12(9):838-840.
11. Saxton MJ & Jacobson K (1997) Single-particle tracking: Applications to membrane dynamics. *Annu Rev Bioph Biom* 26:373-399.
12. Gillespie DT (1977) Exact Stochastic Simulation of Coupled Chemical-Reactions. *Abstr Pap Am Chem S* 173(Mar20):128-128.
13. Raj A, Peskin CS, Tranchina D, Vargas DY, & Tyagi S (2006) Stochastic mRNA synthesis in mammalian cells. *PLoS Biol* 4(10):e309.